JOURNAL OF GEOPHYSICAL RESEARCH, VOL. 94, NO. C12, PAGES 17,971–17,984, DECEMBER 15, 1989

# Global Mesoscale Variability From the Geosat Exact Repeat Mission: Correlation With Ocean Depth

DAVID T. SANDWELL[1] AND BOHAI ZHANG

*Center for Space Research, University of Texas at Austin*

We have developed a new technique for extracting global mesoscale variability from satellite altimeter profiles having large radial orbit error (~3 m). Long-wavelength radial orbit error, as well as other long-wavelength errors (e.g., tides, ionospheric-atmospheric delay, and electromagnetic bias), are suppressed by taking the derivative (slope) of each altimeter profile. A low-pass filter is used to suppress the short-wavelength altimeter noise ($\lambda$ < 100 km). Twenty-two repeat slope profiles are then averaged to produce a mean sea surface slope profile having a precision of about 0.1 μrad. Variations in sea surface slope, which are proportional to changes in current velocity, are obtained by differencing individual profiles from the average profile. Slopes due to mesoscale dynamic topography are typically 1 μrad (i.e., a 0.1-m change in topography over a 100-km distance). Root-mean-square (rms) slope variability as low as 0.2 μrad are found in the southeast Pacific, and maximum slope variations up to 6–8 μrad are found in major western boundary currents (e.g., Gulf Stream, Kuroshio, Falkland, and Agulhas) and Antarctic Circum-polar Current (ACC) systems. The global rms variability map shows previously unknown spatial details that are highly correlated with seafloor topography. Over most areas, the rms slope variability is less than 1 μrad. However at mid-latitudes, areas of higher variability occur in deep water (> 3 km) adjacent to continental shelves, spreading ridges, and oceanic plateaus. Variability is low in shallower areas (< 3 km). Along the ACC, the meso-scale variability appears to be organized by the many shallow areas in its path. We do not see convincing evidence that variability is higher downstream from topographic protrusions. Instead, the areas of highest variability occur in the deep basins (> 4 km).

## INTRODUCTION

Satellite altimetry is becoming an important tool for acquiring global, synoptic measurements of the dynamic topography of the oceans associated with currents, eddies and equatorial waves [*Fu*, 1983*a*]. However, to determine the geostrophic circulation at both mesoscales (50–1000 km) and basin scales (1000–10000 km), the slope of the sea surface (relative to the geoid) must be measured to an accuracy of 0.1 μrad or better [*Born et al.*, 1984]. This slope accuracy corresponds to 0.1 m accuracy (or better) topography measurements over a distance of 1000 km. Such high accuracy data are not yet available from the Geos-3, Seasat, or Geosat altimeter missions. The current limitations [*Tapley et al.*, 1982] are the radial orbit error, tide model errors, atmospheric-ionospheric delay, and electromagnetic bias. Moreover, the largest uncertainty in determining absolute dynamic topography is due to inaccuracy of the global geoid models. Thus both the altimeter measurements and the global geoid models must be substantially improved before global dynamic topography can be measured synoptically. The Topographic Experiment (TOPEX)–Poseidon mission (1991 launch) [*Born et al.*, 1984] may achieve the required accuracies. Geoid models with similar high accuracy may be achieved from a spaceborne gravity gradiometer mission [NASA Geodynamics, 1987] or from improved tracking of low-altitude, drag-compensated satellites.

While the current altimeter data are not accurate enough to measure absolute dynamic topography over basin scales, they are sufficiently accurate for mapping mesoscale (50–1000 km) variations in dynamic topography. This is because the radial orbit error primarily consists of wavelengths greater than 10,000 km (= 10 Mm) [*Marsh and Williamson*, 1980] (and see below). In addition, the sea surface slopes associated with mesoscale variability are relatively large (> 1 μrad). By applying a simple along-track derivative method to Geosat altimeter profiles, we show that the signal to noise for some mesoscale features is about 50; slope variations as low as 0.2 μrad can be detected.

The basic techniques for extracting mesoscale variability from satellite altimeter measurements are well established [see *Fu*, 1983*a*]. The methods involve the removal of long-wavelength orbit error and long-wavelength dynamic topography and then the removal of the time-invariant geoid and steady state ocean circulation components of sea surface topography. These methods have been applied to the 3-year GEOS-3 and 3-month Seasat data sets to determine the statistics of the global mesoscale variability.

The simplest method is the "repeat track method," where profiles of mesoscale variability are obtained from repeated altimeter profiles along the same satellite ground track. The repeat profiles are first averaged together. The average profile consists of the geoid, the time-invariant dynamic topography and the average of all of the long-wavelength errors. Individual profiles are then subtracted from the long-term average. Finally, the long-wavelength error (mostly orbit error) is reduced by removing a linear or quadratic polynomial from each profile. The residual profiles reveal variations in sea surface topography (over the averaging time interval) having wavelengths less than the profile length. For example, despite the relatively low accuracy of the Geos-3 measurements, several groups of investigators [*Douglas and Gaborski*, 1979; *Cheney and Marsh*, 1981*a*; *Douglas et al.*, 1983] were able to measure the relatively high amplitude mesoscale variations of Gulf Stream meanders and eddies using this repeat profile method.

A similar technique was applied to Seasat altimeter data on a global basis [*Cheney et al.*, 1983]. Because of improvements in altimeter design, atmospheric delay corrections and orbit precision, Seasat revealed previously unresolved spatial details in the mesoscale variability of the oceans that are generally consistent with historical data [*Wyrtki et al.*, 1976]. One of the surprising results from the analysis of Seasat data was that over most ocean areas the mesoscale variability is quite low (< 40 mm). The smaller areas of high variability are associated with western boundary currents and the Antarctic Circumpolar Current.

[1]Now at Geologic Research Division, Scripps Institution of Oceanography, La Jolla, California.



Paper number 89JC01397.
0148-0227/89/89JC-01397$05.00

In addition to mapping the global-root-mean-square (rms) mesoscale variability, residual Seasat profiles were used to track time varying mesoscale features [e.g., *Cheney and Marsh*, 1981*b*] over the short 3-day repeat cycle of Seasat. While Seasat's 3-day repeat ground track provided good temporal resolution, its spatial resolution (i.e., ~700 km ground track spacing) was sometimes inadequate for tracking small eddies. A mesoscale eddy detected along a single Seasat ground track eventually drifted to the region between ground tracks. The Geosat altimeter, which has been collecting altimeter data along a 17-day repeat cycle for approximately 1.5 years [*Cheney et al.*, 1987*a*], has better spatial resolution (~125 km) but the increased repeat interval results in poorer temporal resolution.

Papers describing the Geosat altimeter mission and the accuracy of the Geosat altimeter data can be found in the *Johns Hopkins APL Technical Digest (The Navy Geosat mission, volume 8, number 2, 290 pp.*, 1987). The primary mission of Geosat (1.5 years) was to map the marine geoid at a high spatial resolution. Upon completion of its primary mission in October 1986, Geosat was placed into a 17-day repeat orbit (Figure 1). To date, this Geosat Exact Repeat Mission (Geosat/ERM) has completed about 40 cycles having ground tracks that repeat to within about 1 km band across track. One of the more remarkable results from these data is a sea level time series over a large region of the equatorial Pacific showing the propagation of a Kelvin wave associated with the 1986–1987 El Niño [*Cheney et al.*, 1987*b*; *Miller et al.*, 1987]. Sea surface slopes associated with this Kelvin wave range from only 0.04 μrad to 0.1 μrad. Despite the very low amplitude of this feature, the Geosat results show agreement with island tide gauges, inverted echo sounders and thermistor chains [*Cheney and Miller*, 1988]. In our analysis we are primarily interested in mapping the larger-amplitude features (0.1–10 μrad) over all ocean areas including the shallow seas.

Recently, several groups of researchers have computed global mesoscale variability from the first year of the Geosat/ERM data (C. Koblinsky, J. G. Marsh, B. D. Beckley, and Brenner of NASA; L. L. Fu and Zlotnicki of the Jet Propulsion Laboratory; Haxby of Lamont-Doherty Geological Observatory; and D. T. Sandwell and B. Zhang of the University of Texas). These results were presented during the Tenth Geosat Users' Meeting (March 22 and 23, 1988) held at the John's Hopkins Applied Physics Laboratory in Laurel, Maryland. In areas where mesoscale variability is high, the Geosat maps (1-year data span) show higher variability than the Seasat maps (25-day data span) [*Koblinsky*, 1988]. Moreover, the better spatial resolution of Geosat/ERM profiles (compared with Seasat profiles) resolves some interesting details in mesoscale variability. In general, the four research groups presented similar global mesoscale variability maps, suggesting that the results are relatively insensitive to the analysis methods used.

Here we present a simple derivative filter technique for extracting mesoscale variability from satellite altimeter data having large-amplitude (~3 m), long-wavelength (< 10 Mm) errors; no data adjustments are necessary. We apply this method to the first year (22 repeat cycles) of Geosat/ERM data. The derivative high-pass filter that we have adopted has several advantages over previous filter methods (e.g., removing linear trend from 2000 to 3000-km-long altimeter profiles). The main advantage is that the derivative filter is only two points long so that it produces no edge effects. Thus short profiles (> 200 km) can be included in our analysis. In contrast, the tilt and bias removal technique does not work properly when profiles are less than about 1000 km long because much of the signal is removed in the adjustment. Moreover,

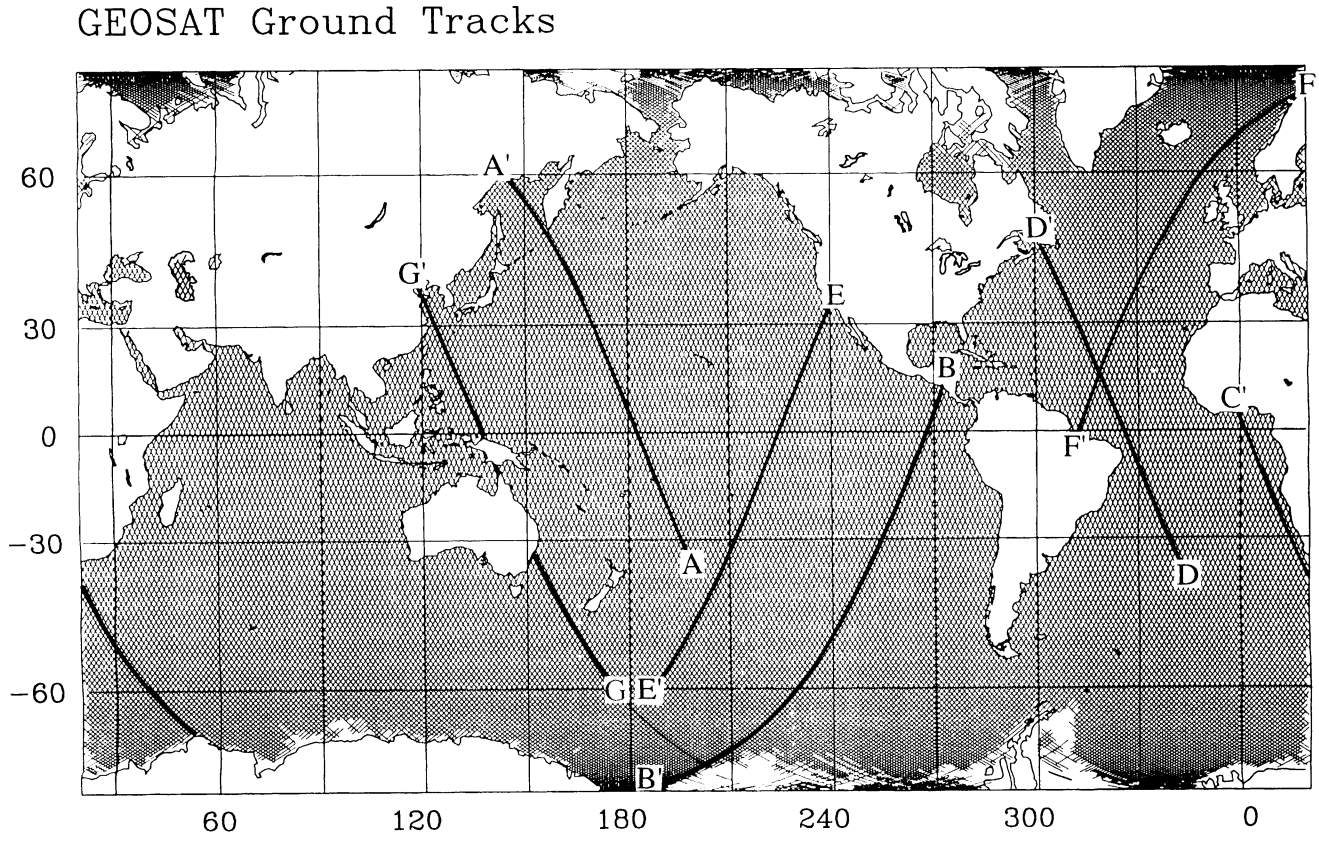


Fig. 1. Ground track for the 17-day repeat cycle of Geosat/ERM. Highlighted profiles A–G are shown in Figures 6 and 7.

we show below that the removal of a tilt and bias from 3000-km-long segments produces small but significant artificial undulations up to 300 km from the ends of each profile. The largest edge effects occur near areas of high variability such as the eastern continental margins of North and South America.

The second advantage of the derivative filter is that it transforms a dynamic height profile into a dynamic slope profile. The dynamic slope of the sea surface (i.e., the difference in dynamic topography at two points divided by the point spacing) is a parameter that can be measured independently. Moreover, if the ocean current is in geostrophic balance, then the dynamic gradient of the sea surface is proportional to the current velocity. There is also a simple relationship between sea surface slope variability and eddy kinetic energy [*Menard*, 1983].

*Douglas et al.* [1984] and *Tai and Fu* [1986] have proposed an improved method of orbit error removal over the conventional "bias and tilt adjustment." In their approach, the radial orbit error of each satellite orbit is estimated globally (rather than regionally over areas a few thousands kilometers on a side) by representing the orbit error as a Fourier series in time. They have shown that the Fourier series representation is preferable because it does not suppress ocean variability with spatial scales less than the shortest wavelength of the Fourier series. It also produces smaller edge effects and forces ascending and descending profiles to agree at crossover points. In comparison with the derivative filter method presented here, the Fourier series method may yield more accurate basin-scale variability but similar mesoscale variability. We have adopted the simple derivative method for this mesoscale study of 180 million new Geosat observations.

## DATA PROCESSING AND ANALYSIS

### *Preprocessing*

The first 22 repeat cycles of the Geosat geophysical data record (GDR) altimeter data from November 7, 1986, to November 16, 1987, were used in our analysis. Each once-per-second GDR includes the following: 10 sea surface height measurements, the average of the 10 measurements, the standard deviation of the average, environmental corrections, and preprocessing flags [*Cheney et al.*, 1987*a*]. On the basis of the previous experience with Seasat altimeter data [*Marsh and Martin*, 1982], the GDRs were edited for the following reasons: flagged data over land or ice; AGC (automatic gain control) greater than 34 dB or less than 15 dB; standard deviation of once-per-second average exceeding 0.1 m and significant wave height (SWH) greater than 8 m. This editing eliminated about 4% of the data.

Instead of using the once-per-second average heights, the 10 per second observations were averaged into twice-per-second observations. The increased sampling rate retains more of the short-wavelength information needed for interpolation and removal of the high-amplitude, short-wavelength geoid undulations (see below). Moreover, we use the average of many repeat cycles for geophysical studies where the short-wavelength information is desired. The following corrections (supplied with the GDRs) were then applied to the twice-per-second data: ocean tides (Schwiderski), solid earth tides (Cartwright), ionosphere delay and troposphere delay (both wet and dry components from the Fleet Numerical Ocenographic Center (FNOC)). After the corrections were applied, the data were divided into ascending or descending passes depending on the sign of the latitude component of satellite velocity. The passes were further subdivided whenever a time gap exceeded 10 s.

### *Orbit Error Analysis*

The major limitation in using Geosat/ERM data for measuring dynamic topography is long-wavelength radial orbit error. The Geosat/ERM orbit was computed by the Navy Astronautics Group (NAG) using the GEM-10 gravity model [*Lerch et al.*, 1981] and Doppler tracking data from the four Transit OPNET tracking stations (all in the United States). Because of gravity model error, the poor geometry of the tracking network combined with the relatively short arcs used in the solutions, and a possible mislocation of the Earth's center of mass [*Haines et al.*, 1990], the NAG radial orbit error is quite large (~5) and it is dominated by a frequency of once per revolution (~40 Mm wavelength) [*Smith et al.*, 1988].

To illustrate this orbit error, three ascending Geosat repeat profiles, crossing the northwestern Pacific (track labeled A–A' in Figure 1), are shown in Figure 2*a*. Two different orbits were used to calculate the profiles. The first was the standard NAG orbit and the second was the CSR (University of Texas, Center for Space Research) orbit computed using a new gravity model (PTGF3A) as well as 80 days of Tranet Doppler tracking data from a global network of 48 stations [*Smith et al.*, 1988]. The differences between the NAG profiles and the CSR profiles are large (~5 m) and mostly reflect the radial component of the NAG orbit error; the CSR orbit is accurate to about 0.35 m. In addition to the large differences between the NAG profiles and the CSR profiles there

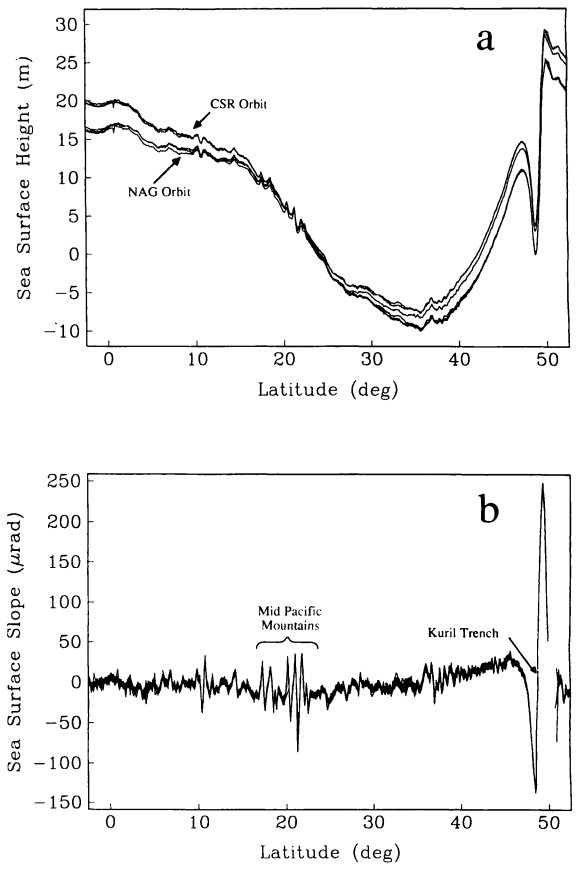


Fig. 2. Three Geosat repeat profiles along ground track A–A' in Figure 1. (*a*) Sea surface height along the three profiles where calculated using the NAG orbit supplied with the data and a more accurate CSR orbit. The absolute orbit error (NAG profile - CSR profile) is about 5 times greater than the relative orbit error (NAG profile - NAG profile). (*b*) Sea surface slope along the three ERM profiles. The derivative suppresses the long wavelengths including the orbit error. Large variations in slope reflect seafloor topography.

are smaller differences among the three profiles having common orbit type, NAG or CSR. This smaller, relative orbit error is ~1.5 m for the NAG profiles and ~0.16 m for the CSR profiles [*Zhang*, 1988]. When the absolute dynamic topography is measured with a satellite altimeter, the absolute radial orbit error limits the accuracy of the measurements. Similarly, when changes in dynamic topography are measured, the accuracy is limited by the relative orbit error. The profiles shown in Figure 2*a* suggest that Geosat/ERM profiles will be best for variability studies where changes in dynamic topography are measured.

To determine the amplitude and dominant wavelengths of the absolute NAG orbit error, we calculated the amplitude spectrum of the difference between the NAG profiles and the CSR profiles for 56 orbit revolutions of data. Since there are numerous large gaps in the data associated with the continents, a least squares technique was used to fit the sine and cosine components one frequency at a time. The spectrum (Figure 3*a*) has a peak of about 5 m at a wavelength of 40 Mm (i.e., one cycle per orbit revolution). A second smaller peak occurs at a wavelength of 20 Mm (twice per revolution). The amplitude spectrum decreases for wavelengths less than 10 Mm, suggesting that the absolute orbit error is small at short wavelengths. Because of these large, long-wavelength errors, the unadjusted Geosat/ERM data cannot be used for oceanographic studies, since the magnitude of the dynamic topography is generally less than 2 m.

One way to suppress the long-wavelength orbit error without adjusting the data is to take the along-track derivative of each profile. As shown in Figure 2b, differentiation suppresses much of the long-wavelength geoid undulation as well as the long-wavelength radial orbit error. In the wave number domain, the derivative corresponds to multiplying the spectrum by $2\pi i/\lambda$ where $\lambda$ is the wavelength. Long wavelengths are suppressed, while short wavelengths are enhanced; the factor $i$ shifts the phase of the signal by 90°. Figure 3*b* (light curve) shows the slope error spectrum for the NAG profiles minus the CSR profiles. The slope spectrum has a peak (~0.8 μrad) at a wavelength of 40 Mm and a smaller peak of ~0.2 μrad at a wavelength of 20 Mm. These results suggest that the absolute slope of the sea surface can be measured to an accuracy of ~1 μrad (e.g., 1 m over 1 Mm) using Geosat/ERM data. In some energetic areas of the oceans, the dynamic topography is 3–8 μrad. Thus the simple differentiation procedure transforms data that are useless for ocean circulation studies into data that are marginally useful for these studies. However, for basin-scale circulation studies the absolute errors in Geosat/ERM data are still 10–100 times too large.

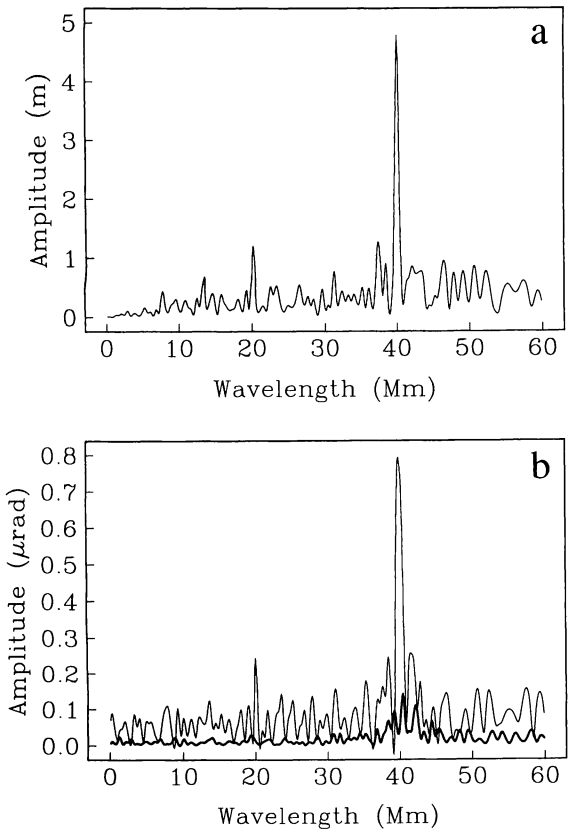


Fig. 3. Amplitude spectrum of radial orbit error. (*a*) The absolute height orbit error spectrum (NAG - CSR) has a peak of ~5 m at 40 Mm wavelength (one cycle per orbit revolution) and a smaller peak ~1 m at 20 Mm wavelength (two cycles per revolution). (*b*) The absolute slope orbit error spectrum (NAG - CSR, light curve) has a peak of 0.8 μrad at 40-Mm wavelength. The relative slope orbit error spectrum (NAG - NAG, dark curve) has a small peak of only 0.15 μrad at 40-Mm wavelength.

The situation is greatly improved when unadjusted Geosat/ERM slope profiles are used for mesoscale variability studies. This is because the relative error in the NAG orbit is smaller than the absolute error, especially at a wavelength of 40 Mm. Much of the error in the NAG orbit appears as a shift in the coordinate system with respect to the Earth's center of mass [*Zhang*, 1988]. These errors repeat geographically and thus are common to repeating profiles. To determine relative slope error, we calculated the spectrum of the difference between the second Geosat/ERM repeat cycle and the average of the 22 repeat cycles. The amplitude spectrum for 71 orbit revolutions is shown in Figure 3*b* as a heavy line. In general, the relative error in the NAG slope spectrum is about 5 times less than the corresponding absolute error. A broad, low- amplitude peak in the relative slope spectrum (0.14 μrad) occurs at a wavelength of 40 Mm. At other wavelengths, the relative error is less than 0.05 μrad. These results show that the relative error among repeat Geosat/ERM slope profiles is only 0.1 to 0.2 μrad. In other words, a 0.2-m change in sea surface topography over a distance of 1000 km can be measured with Geosat/ERM data without adjusting the data.

### *Averaging, Differencing, and Filtering*

After the profiles were edited, corrected, and differentiated, all 22 repeat cycles (~32 million observations) were loaded into two compact files, one for the ascending profiles and the other for the descending profiles. Each file has 244 columns representing the 244 equator crossings and 7000 rows representing the possible number of twice-per-second samples in a complete ascending or descending arc. A third dimension was used to store the 22 repeat cycles. Preprocessed slope profiles were interpolated onto the uniform along-track bins and placed in the file. Because we oversampled the data (i.e., two points per second), a linear interpolation scheme could be used after the data were low-pass filtered (30 km half-amplitude, cutoff wavelength). To avoid storing latitude and longitude information, simple formulas (based on a circular orbit about a rotating elliptical Earth) were used to map the record position into time, geodetic latitude and longitude and vice versa; profiles were assumed to be collinear. After all of the data were loaded into the file, the slopes were averaged when more than six repeat cycles were available. To remove remaining outliers, individual slopes were compared with the average. If an individual slope was more than 5 standard deviations from the average, then it was edited and the average was recomputed. This procedure removed 0.8% of the data. We found this final editing step to be

quite important although it requires that all 22 unfiltered repeat cycles reside on computer disk simultaneously. The average profile was extracted for marine geophysical studies and also subtracted from the individual repeat cycles.

The final step in the processing was to low-pass filter the slope difference profiles. This is necessary because the derivative filter enhances the very short wavelength altimeter noise. The 22 differenced profiles (bottom of Figure 4) were low-pass filtered using a Gaussian filter [$\exp(-t^2/2\sigma^2)$] with $\sigma$ = 1.0 s. This corresponds to a (half amplitude) cutoff wavelength of 30 km. Increasing the filter length reduces the short-wavelength altimeter noise and reveals the mesoscale variability of the Kuroshio as well as the low variability at 10°N. After examining data from many areas, we adopted $\sigma$ = 5.0 s as the filter length (150 km half-amplitude cutoff wavelength). As shown by *Fu* [1983*b*] the mesoscale variability has very little power at wavelengths less than 150 km. To avoid possible edge effects caused by the low-pass filter, 15 s of data (i.e., 100 km) were eliminated from the ends of the profiles.

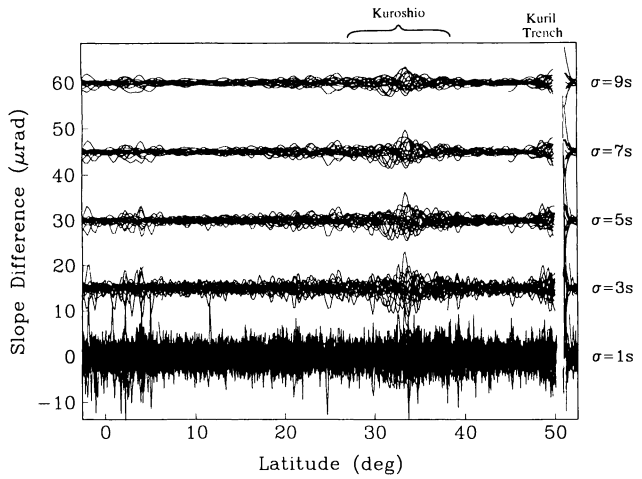


Fig. 4. Twenty-two slope difference profiles along ground track A–A'. Slope differences consist of altimeter noise and mesoscale variability. Altimeter noise was suppresses with a Gaussian-shaped low-pass filter that attenuated 150-km wavelength signals by 0.5 ($\sigma$ = 5 s).

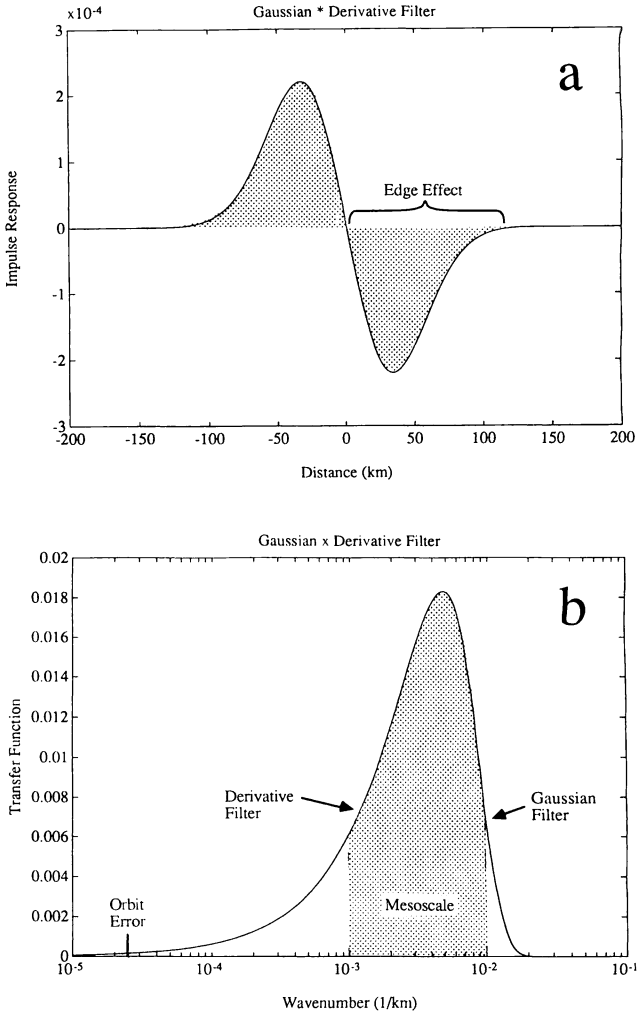


Fig. 5. (*a*) Impulse response function of the derivative and Gaussian filters applied to Geosat/ERM profiles. (*b*) The transfer function, imaginary part, has a peak at 600 km wavelength and passes wavelengths in the 100 to 1000 km band (mesoscale). Radial orbit error is attenuated by -36 dB (i.e., a factor of 66) with respect to the attenuation at 600 km wavelength. The filter is applied by convolving the impulse response function (a) with the profiles. Edge effects are only 100 km.

The transfer function and impulse response function of the combined derivative/low-pass filter are shown in Figure 5. The derivative filter enhances the short wavelengths and suppresses the long wavelengths (Figure 5*a*). For example, radial orbit error having a dominant wavelength of 40 Mm is suppresses by a factor of 100 with respect to a 400-km wavelength signal. The low-pass Gaussian filter attenuates wavelengths of less than about 100 km. The overall transfer function passes signals with wavelengths ranging from 100 km to 1000 km (i.e., the mesoscale). An important aspect of this band-pass filter is that the length of its impulse response is entirely governed by the length of the low-pass filter; in this case the edge effect is only 100 km long (Figure 5*b*).

The repeat profile method assumes that the profiles are collinear. If they are not, then cross-track geoid gradients introduce false signals in the difference profiles. The amplitude of the false signal is equal to the cross-track gradient times the spacing between profiles. Geosat/ERM profiles repeat within about ± 500 m band. The largest geoid gradients are associated with oceanic subduction zones. For example, the Kuril Trench (Figure 2*b* at 48°–50°N) has a geoid gradient of about 300 μrad. The expected amplitudes of false signals above the Kuril Trench are about 0.1 m. In terms of slope this corresponds to ~3 μrad (i.e., 300 μrad slope difference × 500 m band / 50 km distance between slope peak and trough). As expected, these false signals are seen in the difference profiles (Figure 4) at the location of the Kuril Trench axis. Since all ocean trenches have the large geoid gradients, one must be careful when interpreting mesoscale variability in these areas. Over other tectonic features, such as passive continental margins and seamounts, the geoid gradients rarely exceed 100 μrad [*Sandwell*, 1984] so noncollinearity is less of a problem in these areas.

## SLOPE VARIABILITY

### *Slope Difference Profiles*

The variability apparent in the slope difference profiles ranges in amplitude, wavelength, and cause; most but not all of the variability is due to oceanography. To illustrate this variety of signals and their different sources, we plotted the 22 slope difference profiles along seven long satellite passes (Figure 6, profiles A–G). The locations of these seven profiles are marked in Figure 1. For

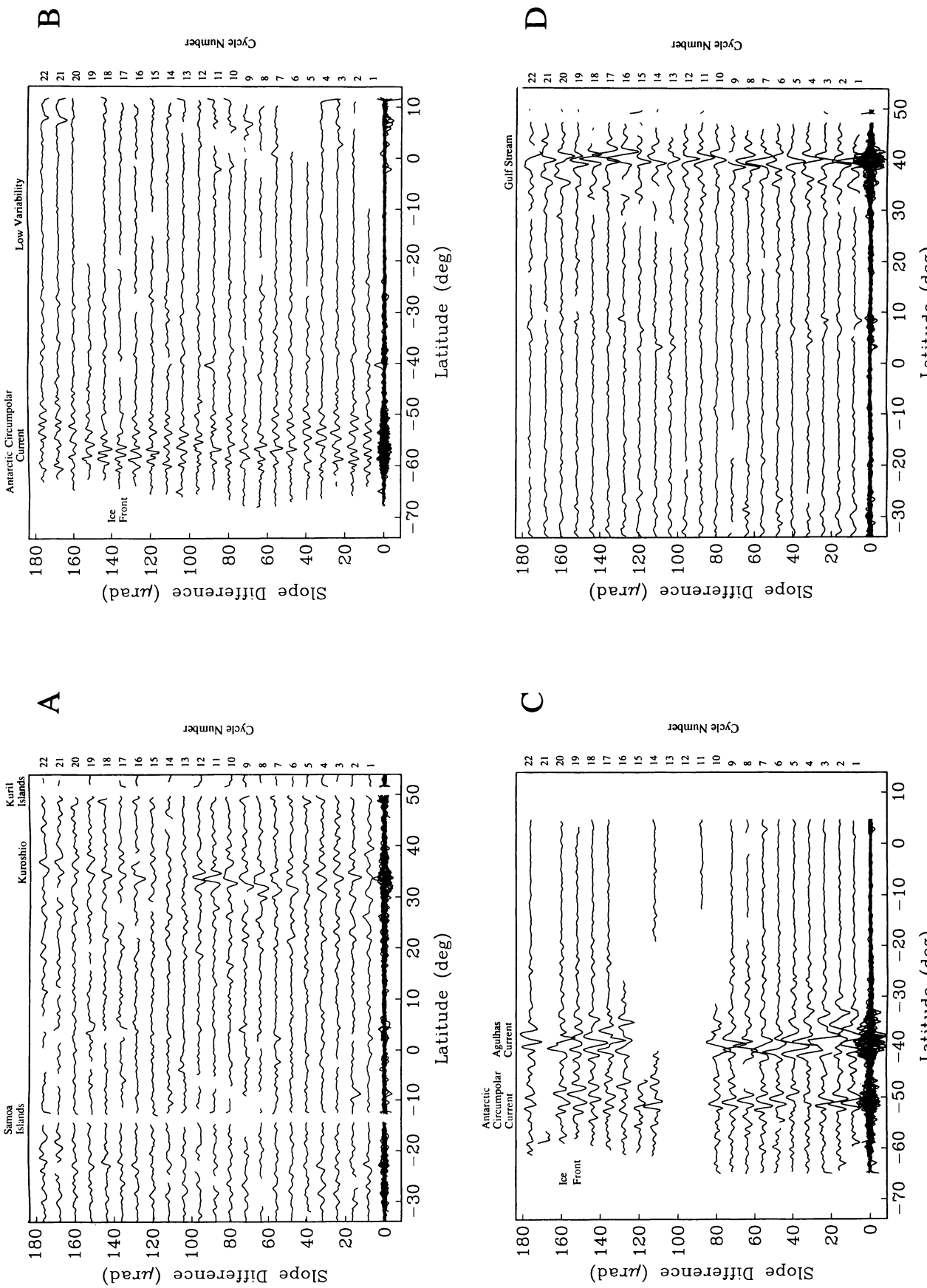


Fig. 6. Twenty-two slope difference profiles along ground tracks A–G shown in Figure 1. The 22 profiles are shown along the bottom of each plot. Successive repeat cycles are also stacked. Significant oceanographic or geophysical features are marked along the top of each plot.

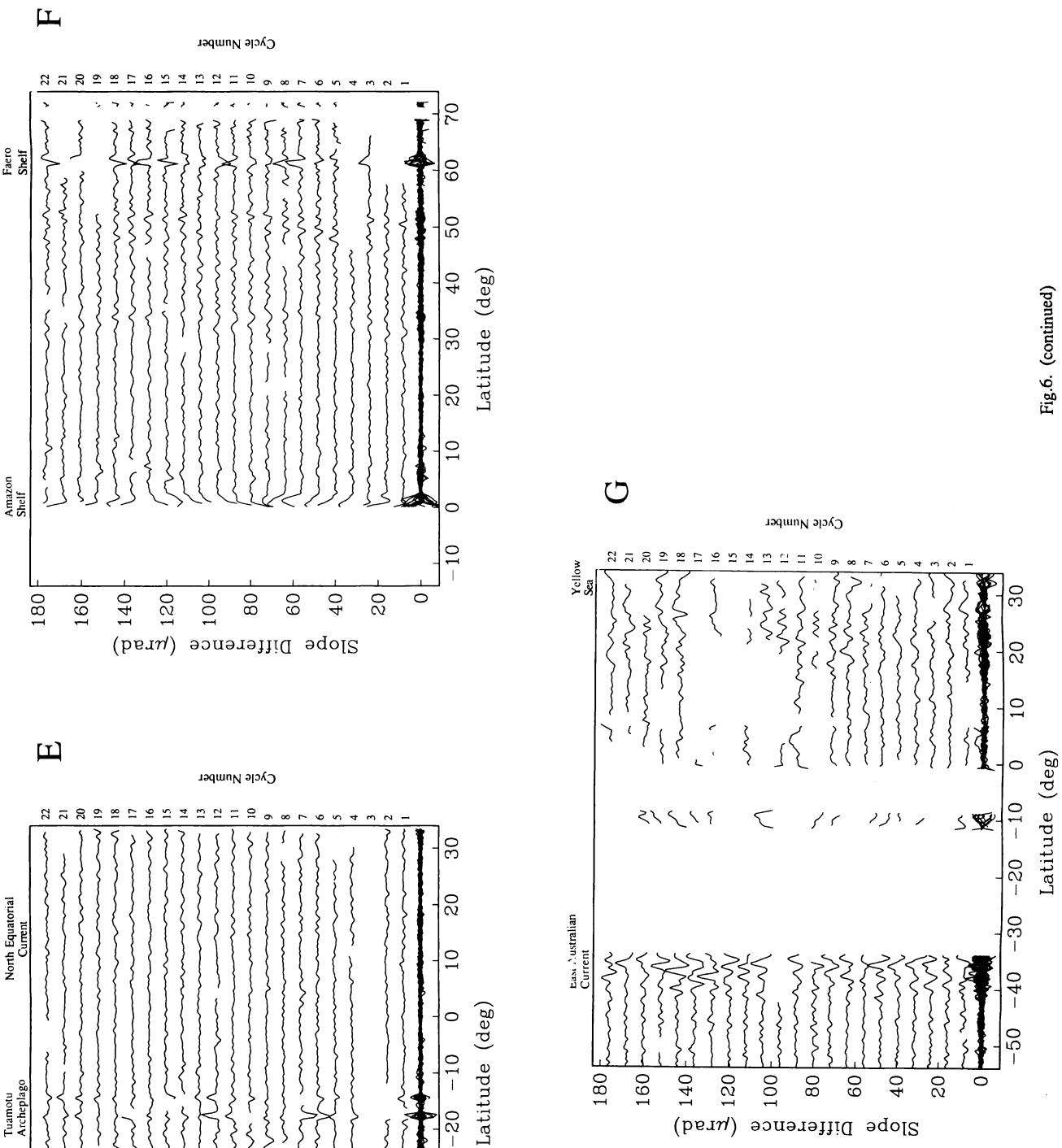


Fig.6. (continued)

example, the ascending profile A–A' crosses the western Pacific in a northwesterly direction and corresponds to the profiles shown in Figures 2 and 4. All 22 repeat profiles are plotted together along the lowest edge of the figure and then they are plotted individually moving up from the bottom of the figure. Two areas of higher variability are apparent in slope difference profile A; one is between -30° and -20° latitude and the other area is between 30° and 40° latitude (i.e., the Kuroshio). Data gaps, associated with the Samoa Islands and the Kuril Islands, are also apparent. In contrast to the tilt and bias method or other types of high-pass filtering techniques, the derivative filter does not produce edge effects. Thus variability can be mapped in areas where many of the repeat cycles are intermittent or missing.

Profile B is a descending profile that extends from the coast of Nicaragua to the Ross Sea (see B–B' in Figure 1). This profile was selected because it crosses an area of extremely low variability (~0.2 μrad) in the southeast Pacific (0° to -20° latitude). This minimum variability is only slightly greater than the long-wavelength orbit error so the actual variability is either at the threshold or below the measurement precision of our unadjusted slope data. At -30° latitude the variability increases to about 1 μrad. The high variability (1–3 μrad) between -48° and -62° is in the vicinity of the Antarctic Circumpolar Current (ACC). The repeat cycles also illustrate the seasonal variation in the Antarctic ice front which is minimal during repeats 7 and 8 and maximal during repeats 18 and 19.

Ascending profile C crosses high-variability areas at both the ACC at ~-50° and the Agulhas Current at ~-40°. Again the variability is very low between -20° and 0°.

Profile D illustrates the high variability (up to ± 8 μrad) of the Gulf Stream at 40° and the correlation of variability with ocean depth. In this area of the Gulf Stream, high variability is expected, but there is an sharp decrease in variability that occurs at 43° latitude. This sharp decrease corresponds to the continental margin where ocean depths decrease from 5 km to 3 km (Figure 7); the transition from high to low variability occurs at an ocean depth of ~4 km. As shown below in greater detail, this correlation of high variability in deep water (3–6 km) and low variability in shallower water (1–3 km) is a global phenomenon at middle and high latitudes.

It is interesting that the correlation of variability and ocean depth has not been noted in previous studies using Geos-3 and Seasat altimeter data. The main reason the correlation was not observed in the Seasat studies was that the spacing of the Seasat profiles (930 km at the equator) was too wide to resolve changes in variability along the narrow (~300 km) continental margins. A secondary reason is that the adjustment of the altimeter profiles causes the variability to "leak" from the high areas into the low areas. The problem is usually exaggerated because areas of high variability occur near continental margins and coastlines where profiles end.

Profile D–D', which crosses the high variability of the Gulf Stream before ending on the shallow continental margin, is used to illustrate the leakage problem (Figure 7). Nine continuous profiles (3000 km long) were chosen for the demonstration (repeat cycles 3–8 and 10–12). The slope profiles and rms slope variation are shown in the middle panel. The rms slope variability reaches a maximum of 5 μrad at 40° and a minimum of less than 0.8 μrad on the shallow margin. The top panel (solid curves) shows the height variations with a linear trend removed by the least squares method. The rms height variability (solid curve) reaches a maximum of 0.33 m at 41° and a minimum of less than 0.15 m on the shallow margin. In contrast to the rms slope variability, which decreases toward the ends of the profiles, the rms height variability increases toward the ends of the profiles, especially on the shallow margin. Moreover, for the slope variability the ratio of maximum to minumum is about 6, while this ratio is only about 2.2 for the height variability. The maps of *Cheney et al.* [1983] and *Koblinsky* [1988], which incorporate the tilt and bias method, show about the same ratio of minimum to maximum (~2.5) variability on and off the North American continental shelf. Individual Seasat profiles (Figure 5 from *Cheney et al.* [1983], upper three profiles) also show the same characteristics as seen in the height profiles of Figure 7.

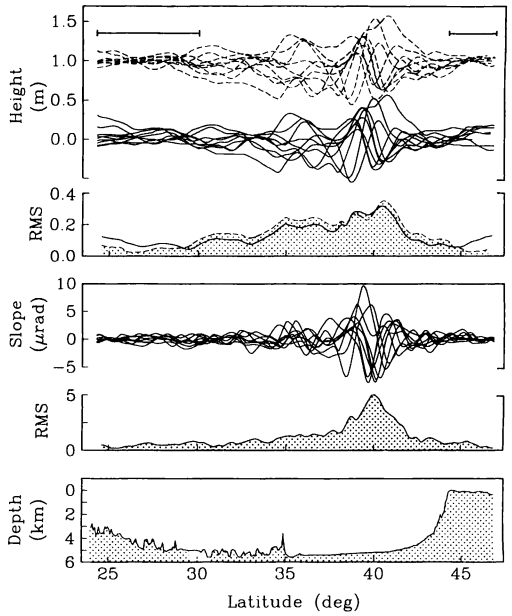


Fig. 7. (Bottom) Seafloor depth, (middle) slope variations, and (top) height variations for ascending profile D–D' which crosses the Gulf Stream and the shallow continental margin (3000 km long). The rms slope variability (middle) is both high and low in the deep ocean (5 km) and low for ocean depths of less than 4 km. Height variability (top) was computed using the tilt and bias method (solid curves), which produces edge effects. Edge effects disappear when higher variability data are excluded from the fit (top, dashed curves).

While height and slope variability are not directly comparable, we believe that the mesoscale variability on the shallow margin is actually about 6 times less than the variability of the Gulf Stream. This suggests that the higher than expected height variability on the continental margin is an edge effect caused by the removal of a linear trend from the height profiles. One way to remedy the problem is to remove the linear trend using only the data in areas where the variability is low. We have applied this method by excluding data between latitudes of 30° and 44° (Figure 7, dashed curves). The rms height variability is now relatively low on the continental shelf (< 0.05 m), and the ratio of maximum to minimum is now 7.2 in better agreement with the slope variability ratio. These combined results indicate that the tilt and bias method of removing long-wavelength orbit error causes artificially high variability near the ends of profiles. Of course, this is exactly the behavior one would expect. The problem is most severe when the variability is high near one end (or both ends) of the profile and less severe when the variability is low near the ends of the profile.

Previous studies show intermediate and sometimes high variability on the shallow continental shelves that are adjacent to areas of high variability such as the Gulf Stream and the Falkland Current. Our analysis suggests the varibility in these areas is actually 2–3 times less than found in previous studies. In the case of the Falkland Plateau, the high variability was attributed to tide model error [*Parke*, 1981]. We believe that the tide models are not especially bad in shelf areas where water depths exceed 200 m. Perhaps this is because the wavelength of the tide model errors is greater than the cutoff wavelength of the high-pass derivative filter (~7000 km at 90% attenuation).

Profile E illustrates a limitation of our method. By adjusting Geosat altimeter profiles (using a crossover method), *Cheney et al.* [1987*b*] were able to map the eastward propagation of a Kelvin wave associated with the 1986–1987 El Niño. Sea surface slopes associated with this Kelvin wave range from only 0.04 μrad to 0.1 μrad. As seen in profile E at 0°, these slopes are too small to be detected using our analysis technique because our accuracies are ~0.2 μrad. However, by gridding and averaging over a 200-km radius (see below), the equatorial variability can be detected but not mapped in detail.

The other feature apparent in profile E is the high variability associated with the very shallow water (< 100 m) of the Tuamotu Archapelago (-15° and -17°). From an examination of several of these anomalous features, we believe that this short-wavelength variability is tide model error. The largest tide model errors appear in water depths of less than 100 m. A more prominent example of tide model error is apparent in profile F where it intersects the Amazon Shelf. On the broad, shallow shelf (depth < 100 m) the sea surface slope profiles vary monotonically from one repeat cycle to the next. Moreover, the signatures seem to repeat themselves after ~20 cycles; cycle 1 looks like cycle 20, 2 looks like 21, and 3 looks like 22. The orbit plane of Geosat precesses at a rate of 1.06° per day with respect to vernal equinox; therefore it takes 340 days to complete one revolution. Every 17.05 days, Geosat returns to the Amazon shelf to sample the solar tide. During this time, the phase of the tide will appear to have shifted by only 18°. After 20 repeat cycles, Geosat will have sampled one complete solar tidal cycle. Although the short-period solar tide is aliased into a much longer period, a long time series of Geosat data could be used to improve tide models in shallow areas where errors are large.

The final profile (G) extends from south of New Zealand, across east Australia and terminates in the Yellow Sea. This profile was included to illustrate the artificially high variability that is associated with missing and/or short profiles. As expected, the variability is high over the East Australian Current (-40° to -35°). However, it is also high along the short profile between northern Australia and New Guinea (-10°). Because Geosat is sometimes unable to regain lock when it moves from land to ocean, only about one half of the data are available over this short segment. In general we find high variability in areas where many profiles are missing (e.g., where land or ice is prevalent). In these areas, some of the high variability is due to poor quality of the available data. However, many of the areas where data are missing are also shallow (< 100 m) so the high variability could be due to tide model error as well.

### *Root-Mean-Square Slope Variability*

The root-mean-square variation in along-track sea surface slope was computed along each track whenever more than 5 of the 22 slope difference profiles were available. Ascending and descending rms slope variations were then averaged into 1° by 1° areas. Areas containing no observations were interpolated from surrounding areas up to 2.7° away. This was done by convolving a Gaussian function (half width 155 km) with only those 1° areas containing data. Areas containing observations were also smoothed by convolving the same Gaussian function with 1° areas that contain data. This two-dimensional, low-pass filter both interpolates and removes wavelengths shorter than 220 km. Along the coastlines, the filter will extrapolate up to 2.7° into the land; a land mask is then applied to eliminate the extrapolated data. The results are shown in Plate 1 and Figure 8 an image of the rms slope variability (Plate 1 can be found in the separate color section in this issue). The colors ranging from violet to red (Plate 1), and gray tone ranging from white to black (Figure 8), indicate the level of variability. Over most ocean areas, the rms slope variability is 1 μrad or less. Small areas of higher variability are associated with mesoscale variations in ocean currents, tide model error, and missing data.

As stated in the last section, the slope variability may become artificially high when many of the repeat cycles are missing. These areas were identified by plotting the number of profiles used to compute the rms slope variation. The data density map is shown in Figure 9 where black represents areas where all 22 repeat profiles are available and white represents areas where there are no profiles. On the average, 15 profiles are available, although there are areas in the Arctic and Antarctic where less than 6 profiles are available. Data from these low-density areas were not used in the rms variability maps.

In ocean areas where the number of profiles is greater than about 6, the rms slope variability reflects mesoscale variations in ocean currents (eddies) as well as unmodelled errors. In general, our results from Geosat/ERM are similar to the mesoscale variability derived from Seasat altimetry [*Cheney et al.*, 1983]. However, this new map has improved coverage because 375 days of Geosat/ERM data were used instead of 25 days of Seasat data. Moreover, spatial resolution is improved because Geosat has a ground track spacing of 160 km instead of the 930 km spacing for Seasat. In addition, because our derivative filter has no edge effects, we were able to extract variations in sea surface slope within 100 km of all shorelines.

The highest variations in sea surface slope (> 3 μrad) occur in the vicinity of the western boundary currents such as the Gulf Stream, the Kuroshio, the Falkland Current, and the Agulhas Current (Plate 1 and Figure 8). The Antarctic Circumpolar Current is associated with a nearly continuous band of medium to high (1.5–4 μrad) variability in the southern ocean. The pattern of ACC variability is not random, but it is highly correlated with the topography of the seafloor. In each ocean the major gyres are delineated by the color contours of rms variability. The highest variability occurs where the western boundary currents depart from the confinement of the continental shelves (30°–50° latitude, Plate 1 and Figure 8). Intermediate variability extends and decreases toward the east and towards the equator. Variability is generally low along the eastern sides of the ocean basins except in the South Atlantic at the Agulhas Retroflection. A band of intermediate to low variability extends across both the Atlantic and Pacific oceans between latitudes of 0° and 15°. The lowest variability (< 0.5 μrad) occurs south of this band in the eastern ocean areas between latitudes of 0° and -30°. The entire Weddell Sea is also characterized by low variability.

### *Correlation with 3-km Depth*

The improved spatial resolution of the rms slope variability map reveals the strong correlation between variability and ocean depth.

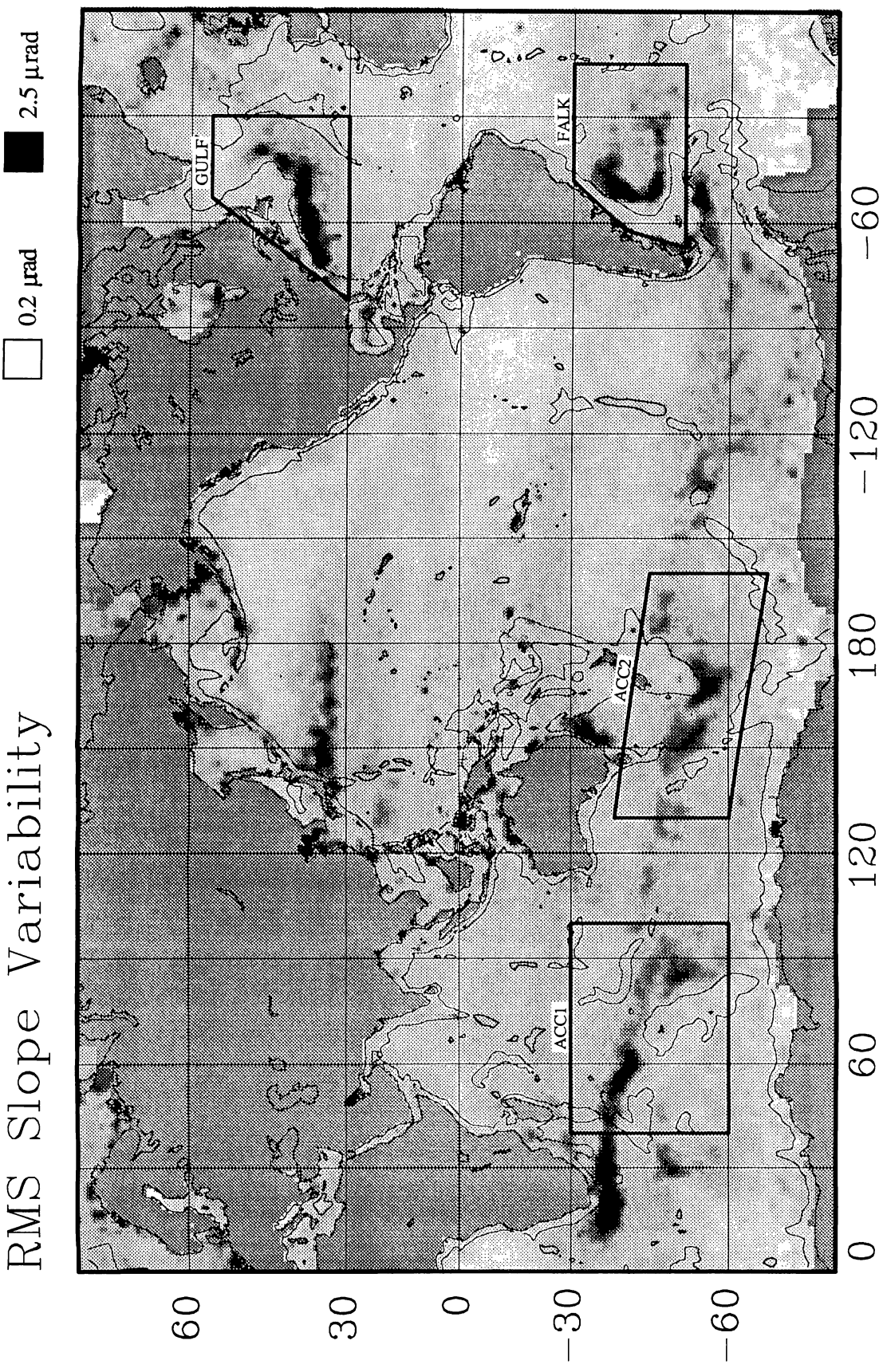


Fig. 8. Plot of rms slope variability for the first year of Geosat/ERM. White is low variability and black is high variability. The 3-km depth contour is also shown. Note the high correlation between variability and seafloor depth. Outlined areas were analyzed in greater detail.

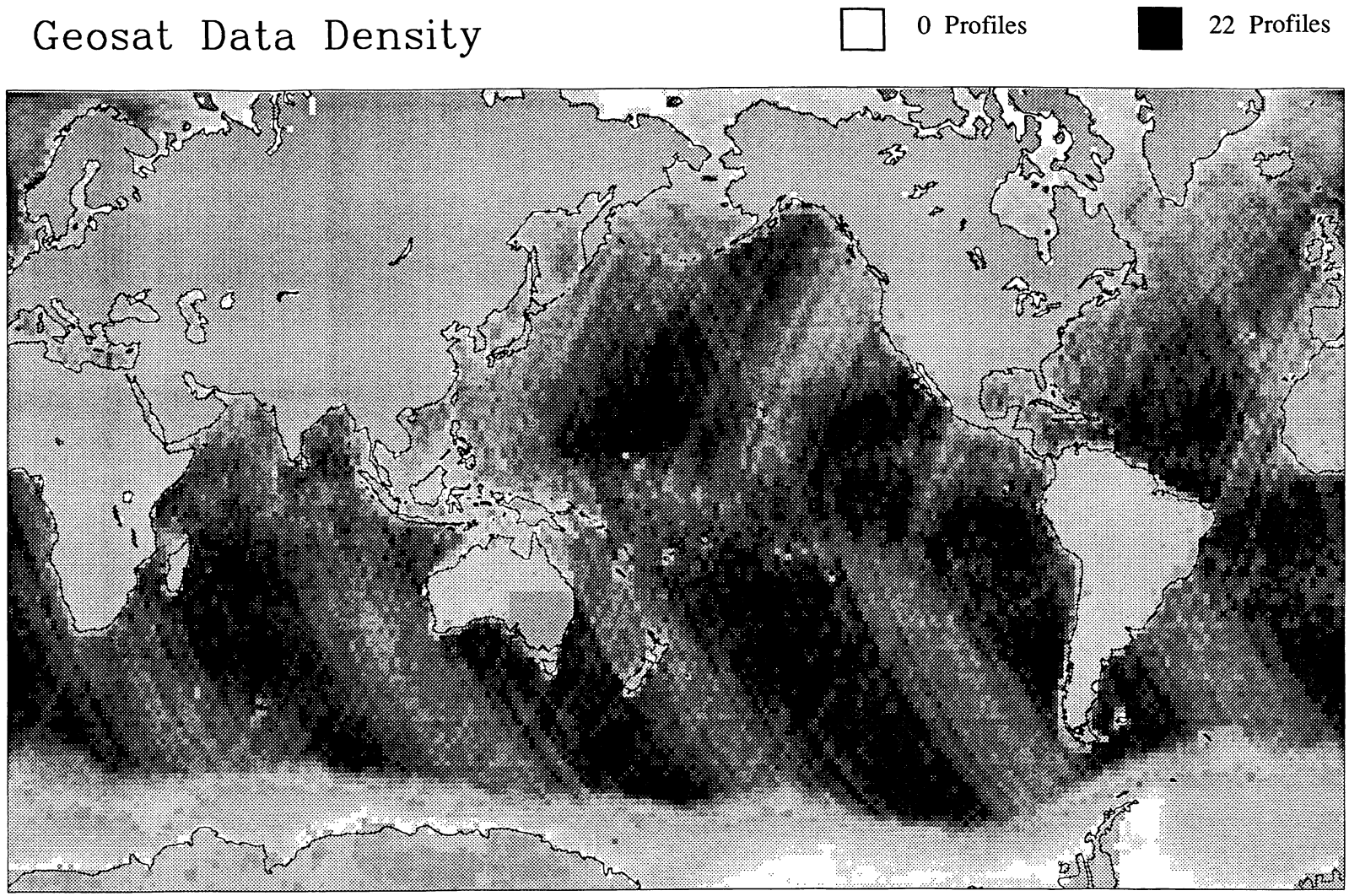


Fig. 9. Density of Geosat/ERM repeat profiles used to construct rms variability maps (white, no data; black, 22 repeat profiles). Low densities occur in polar areas because of seasonal ice cover. Bands of intermediate density are caused by the inability of the radar to regain lock when the attitude of the spacecraft exceeded about 1°.

This correlation is also seen in the absolute dynamic topography maps derived from hydrographic data [e.g., *Gordon and Baker*, 1986]. To show the correlation of mesoscale variability and topography in greater detail, we have plotted the 3-km depth contour on the rms slope variability map (Plate 1 and Figure 8). The 3-km depth contour was derived from a 5-min global topography data base [*Heirtzler et al.*, 1986]. However before contouring, the depths were smoothed and decimated to a 1° by 1° grid using the same Gaussian low-pass filter that was applied to the variability map. Variability is generally high (> 3 μrad) where major ocean currents are strong and ocean depths exceed 3 km. Variability is generally low (< 1 μrad) where ocean depths are less than 3 km, even in areas where currents are intense. High variability also occurs in very shallow water (< 100 m) where ocean tides could be a problem.

The correlation of variability with the 3-km depth contour is most apparent for the western boundary currents and the ACC. For example, Gulf Stream variability increases where the Gulf Stream separates from the continental shelf at North Carolina. To the northeast there is a marked change in variability that coincides with the 3-km depth contour; variability is low on the shallow side of this contour and high on the deep side. At the Grand Banks, the variability pattern turns northward following the deep ocean basin. Further to the east, variability is low over the Mid-Atlantic Ridge, where it is shallower than 3 km. The correlation of bottom topography and eddy migration patterns was reported in many previous studies of mid- to high-latitude eddies (see review by *Gordon and Owens* [1987]). For example, important topographic influences on Gulf Stream eddies were observed in float trajectories near the Blake-Bahama Outer Ridge [*Rossby et al.*, 1983].

The Kuroshio variability does not exhibit this strong correlation with topography because there are only minor, shallow areas in its path. However, variability is low above the Shatsky rise (32°N, 158°E) even though this feature does not protrude above 3 km depth. The Kuroshio variability also ends rather abruptly at 180° where the Kuroshio intersects the Hess Rise (> 3 km deep), in fair agreement with the hydrographic results of *Bernstein and White* [1977].

The variability of the Falkland Current shows an excellent correlation with the 3-km depth contour where variability is high in the deep Argentine Basin and low on the Falkland Plateau. Other correlations of variability with ocean depth occur along the east coast of Australia as well as in the Gulf of Mexico, although these features are not well resolved in our analysis.

The most striking correlation of variability and ocean depth occurs along the ACC. The pattern is similar to the dynamic height anomaly map of the ACC derived from hydrographic data [*Gordon and Baker*, 1986]. Starting at 0° longitude and moving eastward around Antarctica, we find that the variability has intermediate values in the deep South Atlantic but is low above the Southwest Indian Ridge, the Walvis Ridge, and the western continental margin of Africa. Further to the east the variability reaches a maximum in the Agulhas Basin and then is constricted by the narrow passage between the Agulhas Plateau and the South African Margin in agreement with hydrographic and buoy-derived tracks of the Agulhas eddies [*Grundlingh*, 1983]. A second local maximum occurs in the Enderby Basin just south of the Southwest Indian Ridge. The variability at 45° longitude is low above the three major plateaus, the Madagascar Ridge, the Del Caño Rise, and the Conrad Rise. Between the Madagascar Ridge and the Del Caño Rise, the variability appears to be focused by the narrow passage. To the east (60° longitude) another local maximum in variability occurs in the deepest part of the ocean basin (5.5 km deep). Variability is low on the Kerguelen Plateau and the shallow part of the Southeast Indian Ridge and high in the basin between these features. The boundary between high and low variability correlated well with the 3-km depth contour, especially along the northeast margin of the Kerguelen Plateau.

Between 100° and 140° longitude there are no major topographic plateaus and the variability has intermediate values and its pattern is diffuse. However, between 140° and 180° longitude there are a series of topographic barriers that appear to organize the variability. At 150° longitude the variability is low above the Tasman Rise as well as the shallow part of the Southeast Indian Ridge; high variability occurs in the basin between these features. Further to the east, the ACC crosses the narrow Macquarie Ridge which extends from New Zealand in the north to the shallow Southeast Indian Ridge in the south. The variability is intermediate to low above the Macquarie Ridge and increases to the east; a local maximum occurs in the 5 km deep Emerald–Southwest Pacific Basin. In agreement with previous studies [*Colton and Chase*, 1983], we find that the variability is high downstream from the Macquarie Ridge. We also find that variability is high in the basin upstream from the Macquarie Ridge.

Along the Campbell Plateau (170° longitude), the boundary between high and low variability is well correlated with the 3-km depth contour. The high variability follows the deep Southwest Pacific Basin in a northeast direction and then turns eastward across the South Pacific. Variability is lower above the Pacific-Antarctic Rise (2.5 km deep). Further to the east the variability is intermediate and its pattern is diffuse until the ACC reaches the constriction of the Drake Passage. Variability is not especially high in the Drake Passage. However, again we find the highest variability occurs in the deepest water (5 km) along the northern boundary of the Drake Passage. Variability is low in the shallow Scotia Sea but returns to intermediate values when the ACC reaches the deep South Atlantic.

To further illustrate the correlation of mesoscale variability with ocean depth and to confirm that this correlation is primarily a deepwater phenomenon, we have plotted rms slope variability versus depth in four large areas. These areas, outlined in Figure 8, are the northwest Atlantic (GULF), the southwest Atlantic (FALK), the southern Indian Ocean (ACC1) and the southeast Indian and southwest Pacific Ocean (ACC2). In each area, 1° average variability was plotted against 1° average depth (Figure 10). Eighty percent of the data points fall below the solid curves. (The curves were calculated from histograms of 60 adjacent depth points.) In the northwest and southwest Atlantic (GULF and FALK) the 80% level variability is between 1.0 μrad and 1.5 μrad for water depths of less than 4 km. At greater depths (4–6 km) the 80% variability ranges from about 1.5 μrad to 3.0 μrad. The transitition from intermediate to high variability occurs between 4 and 4.5 km depth in these two areas. A similar pattern is observed in the two areas containing the Antarctic Circumpolar Current (ACC1 and ACC2). However, in these two ACC areas the transition occurs at a shallower depth (~3 km) and is less pronounced. Overall, the results show that rms slope variability rarely exceeds 1 μrad when the ocean depth is less than 3 km and that variability is both high and low in the deeper ocean. In several cases, features with minimum depths of 2.5 km (e.g., Mid-Atlantic Ridge, Southeast Indian Ridge) have a major influence on the pattern of mesoscale variability. Thus the correlation of variability with deep water is not related to shallow (< 2 km) areas that are nearby.

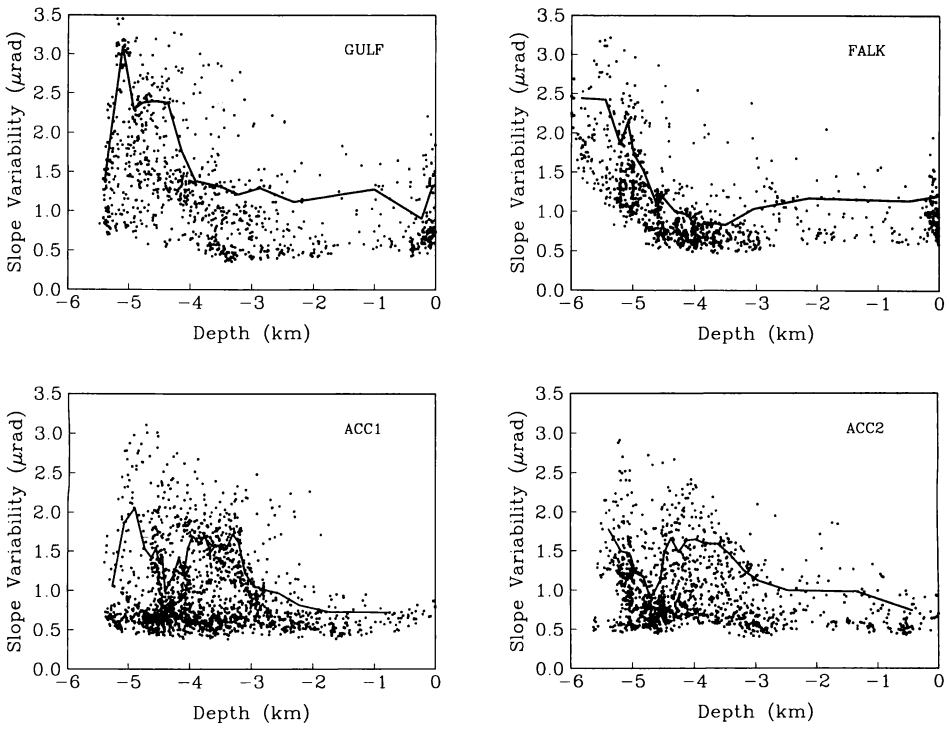


Fig. 10. Plots of rms slope variability (1° by 1° averages) versus seafloor depth for each of the four areas outlined in Figure 8. Eighty percent of the points fall below the solid lines. Variability is both high and low in the deeper ocean and low in the shallower ocean. The transistion between high and low occurs at ~4 km depth for the northwest and southwest Atlantic areas and at ~3 km for the ACC areas.

*Possible Variability Due to Tide Model Error*

As shown in profiles E and especially F (Figure 6), large tide model errors produce variations in sea surface slope, especially in shallow water (< 100 m). These and other shallow-water tide errors are also apparent in Plate 1 and Figure 8. However, one must keep in mind that high variability also occurs in shallow areas near land where many of the repeat profiles are sometimes missing. Thus we focus our observations on areas where most of the repeat profiles are available (Figure 9). Areas of high variability occur over two types of shallow-water features: shallow continental shelves in remote areas and deep ocean seamounts and plateaus that rise to near sea level. The most prominent example of shelf tide model error occurs on the Amazon shelf where water depths are less than 100 m. As shown in profile F of Figure 6, this tide model error is perfectly aliased from a period of 1 day to a period of 340 days by the sampling characteristics of Geosat. We believe (but have not demonstrated) that other less prominent examples of tide model error occur in the Yellow Sea, the Timor Sea (northwest Australia), the Great Barrier Reef (northeast Australia), the southernmost Patagonian shelf, and Bristol Bay (southeast Alaska). While large tide model errors may sometimes occur in shallow shelf areas, there are many broad, shallow shelves where tide model error is not apparent. We speculate that either the tides are well known on these shelves or the short-wavelength tidal variations are low.

The more troublesome shallow-water variability sometimes occurs above shallow seamounts and plateaus that are surrounded by the deep oceans. In these areas, one would expect the tide models to be quite accurate. However, high variability occurs in the shallow parts of the Tuamotu Archapelago (profile E), Marshall Seamounts, St. Helena Island, and the Maldives (Indian Ocean). At each of these features there is only a very small island(s) that protrudes above sea level. There are two probable causes for this high variability. First, the variability is due to radar reflections from the land areas. Second, these small islands do not have tide gauges that were used when developing the tide models. It is important to establish which of these causes the variability. If it is due to land reflections, then one must be more careful in editing land radar returns. If it is true tide model error, then one must work to improve tide models in these small regions.

## SUMMARY

The large absolute radial orbit error for the Geosat/ERM mission (5–10 m) prohibits the use of these data for basin-scale studies of ocean circulation. Most of this large radial orbit error occurs at a period of one cycle per revolution. Moreover, it repeats geographically so that the relative orbit error among repeat profiles is only 1–3 m. In previous studies the tilt and bias method has been used to remove the long-wavelength relative orbit error in order to extract mesoscale (100–1000 km) variations in dynamic topography. Away from the coastline the tilt and bias method is effective and accurate. However, significant edge effects can occur near the ends of profiles where variability is high. The largest edge effects produce artificially high variability (2 to 3 times the actual value) on shallow continental shelves that are adjacent to western boundary currents.

We have developed a simple band-pass filter method in order to suppress the long-wavelength radial orbit error without producing edge artifacts. Each altimeter profile is first differentiated (high-pass filter) and then averaged with the other collinear slope profiles. The next step is to subtract the average profile from the individual repeat profiles. The final step is to suppress the altime-

ter noise with a low-pass filter. The advantages of this method are that no adjustments of the profiles are necessary, and that the high-pass derivative filter produces no edge effects. Short edge effects (< 100 km) are produced by the low-pass filter, so we eliminate the data 100 km from the ends of the passes. A spectral analysis of repeat slope profiles reveals that the largest component of radial orbit error has an amplitude of 0.14 μrad at a wavelength of ~40 Mm. At longer and shorter wavelengths the error is generally less than 0.03 μrad. This maximum relative Geosat/ERM orbit error transformed into slope error corresponds to a measurement error of only 0.14 m over a distance of 1000 km. Since mesoscale slope variability is almost always greater than 0.2 μrad, the simple differentiation procedure effectively suppresses the orbit error below the variability signal.

The global rms variability map shows previously unknown spatial details that are highly correlated with seafloor topography. Over most areas, the rms slope variability is less than 1 μrad. However at middle to high latitudes, areas of high variability occur in deep water (> 3 km) adjacent to continental shelves, spreading ridges and oceanic plateaus. Variability is low in shallow areas (< 3 km). Along the ACC, the mesoscale variability appears to be organized by the many shallow areas in its path. Some of these apparent barriers to variability reach minimum depths of only 2.5 km. We do not see convincing evidence that variability is higher downstream from topographic protrusions. Instead, the areas of highest variability occurs in the deep basins (> 4 km).

*Acknowledgments.* We thank Bob Cheney, Laury Miller, Bruce Douglas, Russ Agreen, Dave Porter, and Nancy Doyle for providing the high-quality Geosat Geophysical Data Records for our study. We thank Steve Nerem, C.K. Shum and Byron Tapley, Bill Haxby, and three reviewers for their helpful comments and suggestions. This work was supported by the Texas Advanced Technology Research Program, the Topex/Poseidon Science Investigation Program (NASA/JPL 958122) and the NASA Geodynamics Program (NAG 5-787).

## REFERENCES

Bernstein, R. L., and W. B. White, Zonal variability in the distribution of eddy energy in the mid-latitude North Pacific ocean, *J. Phys. Oceanogr., 7*, 123–126, 1977.

Born, G. H., C. Wunsch, and C. A. Yamarone, TOPEX: Observing the oceans from space, *Eos Trans. AGU, 65*, 433–434, 1984.

Cheney, R. E., and J. G. Marsh, Ocean eddy variability measured by Geos-3 crossover differences, *Eos Trans. AGU, 62*, 743–752, 1981*a*.

Cheney, R. E., and J. G. Marsh, Seasat altimeter observations of dynamic topography in the Gulf Stream region, *J. Geophys. Res., 86*, 473–483, 1981*b*.

Cheney, R. E., and L. Miller, Mapping the 1986-1987 El Niño with Geosat altimeter data, *Eos Trans. AGU, 69*, 754–755, 1988.

Cheney, R. E., J. G. Marsh, and B. D. Beckley, Global mesoscale variability from collinear tracks of Seasat altimeter data, *J. Geophys. Res., 88*, 4343–4354, 1983.

Cheney, R. E., B. C. Douglas, R. W. Agreen, L. Miller, D. L. Porter, and N. S. Doyle, Geosat altimeter geophysical data record user handbook, *NOAA Tech. Memo., NOS NGS-46*, 29 pp., 1987*a*.

Cheney, R. E., L. Miller, B. C. Douglas, and R. W. Agreen, Monitoring equatorial Pacific sea level with Geosat, *Johns Hopkins APL Tech. Dig., 8*, 245–250, 1987*b*.

Cheney, R. E., B. C. Douglas, and L. Miller, Evaluation of Geosat altimeter data with application to the tropical Pacific sea level variability, *J. Geophys. Res., 94*, 4737–4747, 1989.

Colton M. T., and R. R. P. Chase, Interaction of the Antarctic Circumpolar Current with bottom topography: An investigation using satellite altimetry, *J. Geophys. Res., 88*, 1825–1843, 1983.

Douglas, B. C., and P. D. Gaborski, Observations of sea surface topography with Geos-3 altimeter data, *J. Geophys. Res., 84*, 3893–3896, 1979.

Douglas, B. C., R. E. Cheney, and R. W. Agreen, Eddy energy of the northwest Atlantic and Gulf of Mexico determined from Geos-3 altimetry, *J. Geophys. Res., 88*, 9595–9603, 1983.

Douglas, B. C., R. W. Agreen, and D. T. Sandwell, Observing global ocean circulation with Seasat altimeter data, *Mar. Geod., 8*, 67–83, 1984.

Fu, L. L., Resent progress in the application of satellite altimetry to observing the mesoscale variability and general circulation of the oceans, *Rev. Geophys., 21*, 1657–1666, 1983*a*.

Fu, L. L., On the wave number spectrum of oceanic mesoscale variability observed by the Seasat altimeter, *J. Geophys. Res., 88*, 4331–4341, 1983*b*.

Gordon, A. G., and T. N. Baker, *Southern Ocean Atlas*, plate 232, Amerind, New Delhi, 1986.

Gordon, A. L., and W. B. Owens, Polar oceans, *Rev. Geophys., 25*, 227–233, 1987.

Grundlingh, M. L., Eddies in the southern Indian Ocean and Agulhas Current, in *Eddies in Marine Science*, edited by A. R. Bobinson, chap. 13, Springer-Verlag, New York, 1983.

Haines, B. J., G. H. Born, J. G. Marsh, and R. Williamson, Precise orbit computation for the Geosat exact repeat mission, *J. Geophys. Res.*, in press, 1989.

Heirtzler, J. R., M. Edwards, and A. L. Dilonardo, Relief of the surface of the Earth, Hemispheric Images, *Rep. MGG-2*, map, Natl. Oceanic and Atmos. Admin., Boulder, Colo., 1986.

Koblinsky, C., Geosat vs. Seasat, *Eos Trans. AGU, 69*, 1026, 1988.

Lerch, F. J., C. A. Wagner, and S. M. Klosko, Goddard Earth models for oceanographic applications (GEM 10B and 10C), *Mar. Geod., 5*, 2–43 1981.

Marsh, J. G., and T. V. Martin, The Seasat altimeter mean sea surface model, *J. Geophys. Res., 87*, 3269–3280, 1982.

Marsh, J. G., and R. G. Williamson, Precision orbit analysis in support of the Seasat altimeter experiment, *J. Astron. Sci., 28*, 345–369, 1980.

Menard, Y., Observations of eddy fields in the northwest Atlantic and northwest Pacific by Seasat altimeter data, *J. Geophys. Res., 88*, 1853–1866, 1983.

Miller, L., R. E. Cheney, and B. C. Douglas, Geosat altimeter observations of Kelvin waves and the 1986–87 El Niño, *Science, 239*, 52–54, 1987.

NASA Geodynamics, *Geophysical and Geodetic Requirements for Global Gravity Field Measurements 1987–2000, Report of a Gravity Workshop, Colorado Springs*, 45 pp., Washington, D. C., 1987.

Parke, M. E., Tides on the Patagonian shelf from the Seasat radar altimeter, in *Oceanography From Space*, edited by J. F. R. Gower, pp. 919–926, Plenum, New York, 1981.

Rossby, H. T., S. C. Riser, and A. J. Mariano, The western North Atlantic – A Lagrangian viewpoint, in *Eddies in Marine Science*, edited by A. R. Bobinson, chap. 4, Springer-Verlag, New York, 1983.

Sandwell, D. T., Along-track deflection of the vertical from Seasat, GEBCO overlays, *NOAA Tech. Memo., NOS NGS-40*, 8 pp., 1984.

Smith, J. C., J. C. Ries, C. K. Shum, B. E. Schutz, and B. D. Tapley, Precision Orbit Determination for the Geosat Exact Repeat Mission, *Proc. AIAA-AAS*, 35–45, Astrodynamics Conference August 15-17, Minneapolis, Minn., 1988.

Tai, C. K., and L. L. Fu, On crossover adjustment in satellite altimetry and its oceanographic implications, *J. Geophys. Res., 91*, 2549–2554, 1986.

Tapley, B. D., G. H. Born, and M. E. Parke, The Seasat altimeter data and its accuracy assessment, *J. Geophys. Res., 87*, 3179–3188, 1982.

Wyrtki, K., L. Magaard, and J. Hager, Eddy energy in the oceans, *J. Geophys. Res., 81*, 2641–2646, 1976.

Zhang, B., Geosat/ERM altimeter data analysis for the determination of global oceanic mesoscale variability, Ph. D. thesis, 155 pp., Univ. of Tex., Austin, 1988.

D. T. Sandwell, Geologic Research Division, A-020 Scripps Institution of Oceanography, La Jolla, CA 92093.

B. Zhang, Center for Space Research, University of Texas at Austin, Austin, TX 78712.

(Received October 28, 1988;
revised June 15, 1989;
accepted June 19, 1989.)

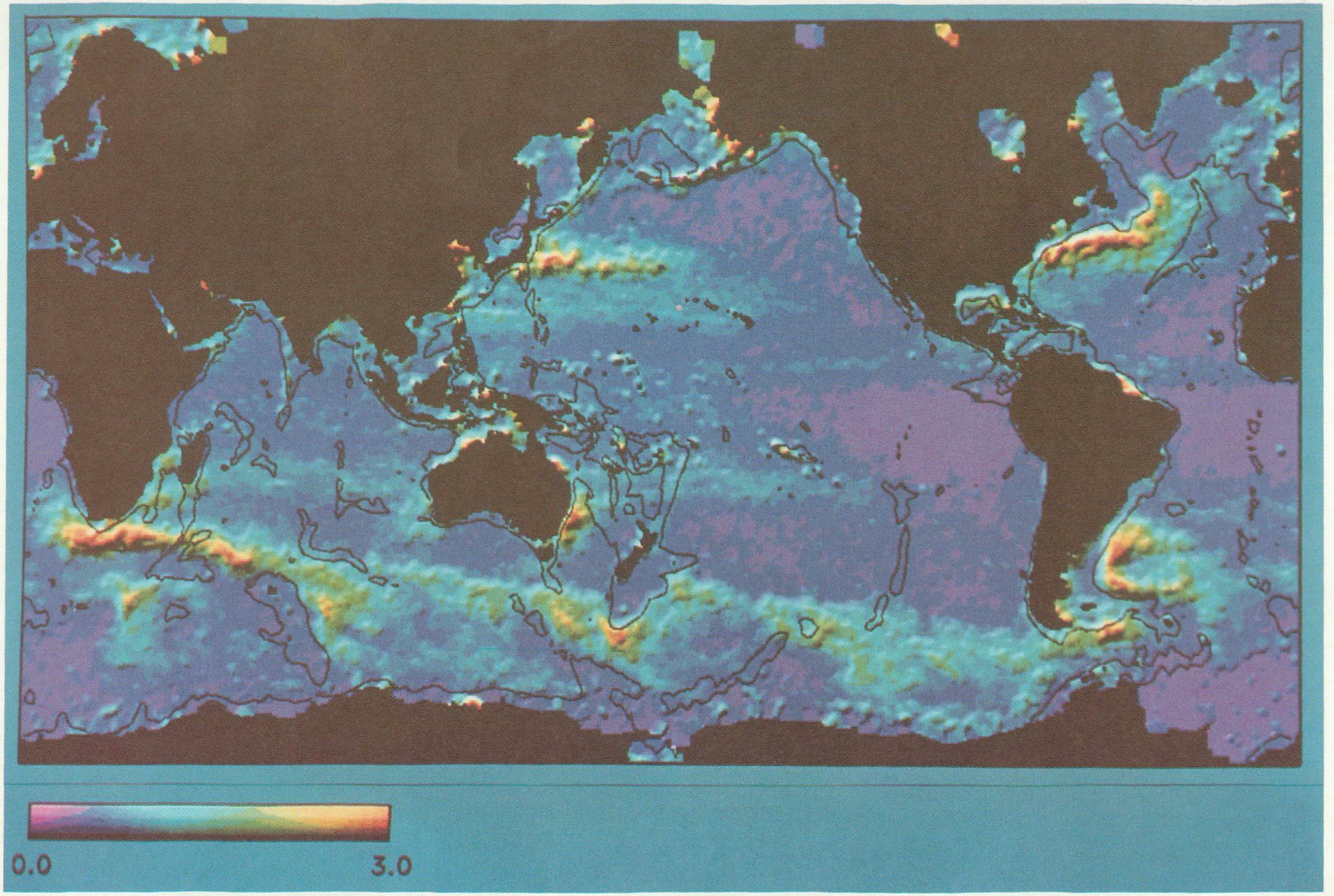


Plate 1. Root-mean-square (rms) slope variability from 1 year of Geosat/ERM data. Violet and dark blue represent low (< 1 μrad) variation in sea surface slope, and red represents high (> 3 μrad) variations in slope. Over most ocean areas the rms variability is less than 0.7 μrad. Zonal bands of intermediate variability are associated with the major gyres and equatorial currents. The highest variability occurs in the western boundary currents and the Antarctic Circumpolar Current. The contour marks 3 km ocean depth. Note the high correlation between variability and ocean depth. Variability is usually low when the ocean depth is less than 3 km and sometimes high when depths exceed 3 km. Along the ACC the highest variability occurs in basins where depths exceed 4 km. Areas of high variability (tide model error) also occur on the very shallow (< 100 m) continental shelves.